Research Article Vol. 13, No. 10 / October 2025 / Photonics Research 2903

PHOTONICS Research

Optical intensity-gradient torque due to chiral multipole interplay

Jiquan Wen,[1] Huajin Chen,[1,2,3,7] Hongxia Zheng,[1,2,3,8] Shaohui Yan,[4] Baoli Yao,[4] Olivier J. F. Martin,[5] Xiaohao Xu,[4,5,9] and Zhifang Lin[2,6]

[1]School of Electronic Engineering, Guangxi University of Science and Technology, Liuzhou 545006, China
[2]State Key Laboratory of Surface Physics and Department of Physics, Fudan University, Shanghai 200433, China
[3]Guangxi Key Laboratory of Multidimensional Information Fusion for Intelligent Vehicles, Liuzhou 545006, China
[4]State Key Laboratory of Transient Optics and Photonics, Xi'an Institute of Optics and Precision Mechanics, Chinese Academy of Sciences, Xi'an 710119, China
[5]Nanophotonics and Metrology Laboratory (NAM), Swiss Federal Institute of Technology Lausanne (EPFL), Lausanne 1015, Switzerland
[6]Collaborative Innovation Center of Advanced Microstructures, Nanjing University, Nanjing 210093, China
[7]e-mail: huajinchen13@fudan.edu.cn
[8]e-mail: hxzheng18@fudan.edu.cn
[9]e-mail: xuxhao_dakuren@163.com

Received 29 April 2025; revised 7 July 2025; accepted 9 July 2025; posted 16 July 2025 (Doc. ID 566257); published 1 October 2025

Owing to the ubiquity and easy-to-shape property of optical intensity, the intensity gradient force of light has been most spectacularly exploited in optical manipulation. Manifesting the intensity gradient as an optical torque to spin particles is of great fascination on both fundamental and practical sides but remains elusive. Here, we theoretically predict the existence of the optical intensity-gradient torque in the interaction of light with chiral particles. Such a new type of torque derives from the interplay between chirality-induced multipoles, which switches its direction for particles with opposite chirality. We show that this torque can be directly detected by a simple standing wave field, created with the interference of two counterpropagating plane-like waves. Our work offers a unique route to achieve rotational control of matter by tailoring the field intensity of Maxwell waves, demonstrated through three-dimensional spinning of a trapped chiral particle. It also establishes a framework that maps a remarkable connection between the optical forces and torques, across chiral to non-chiral.

https://doi.org/10.1364/PRJ.566257

1. INTRODUCTION

An ongoing endeavor in optomechanics is to achieve accurate, on-demand control of minute particles for advanced applications in imaging, precise measurements, and sensing [1–5]. Central to this endeavor is to understand optical forces and torques in a way traceable to the structure of light and particle properties. When light impinges on a particle, optically excited multipoles interact with the excitation field and themselves, giving rise to interception (or extinction) and recoil (or scattering) mechanical effects, respectively [6–10]. In these interaction processes, the optical force may be produced by the intensity gradient [7,11], and other field properties such as the phase gradient [12], momentum, and reactive or imaginary Poynting momentum (IPM) [7,9,13,14], which complement the translational control of the particle. Akin to the force, the optical torque is associated with both light extinction and scattering, but the interplay between different-type multipoles does not contribute to the angular momentum transfer [8,15], which prevents a spectrum of field quantities from being coupled to the torque on normal particles. Consequently, the generation of a torque has relied heavily on the optical spin [1,16–19], the magnitude of which is limited by the intensity.

Exploiting particle chirality would open unexpected opportunities for optical manipulation [20–22]. This has been demonstrated for dipolar chiral particles, on which the kinetic momentum manifests itself as a torque [23–25], with important applications in enantiomer identification. The main aim of this paper is to ask whether the torque can be induced by the intensity inhomogeneity, which was previously considered responsible only for the force. We demonstrate, analytically and numerically, the existence of such intensity-gradient torque for chiral particles, which descends from the recoil effects and exhibits an anti-asymmetry with respect to the electric and magnetic responses of the particle. Also, three-dimensional (3D) rotation of chiral particles is demonstrated utilizing an interference field arising from two counterpropagating Gaussian beams, as illustrated in Fig. 1. We also present a general framework for classifying the optical torques according to

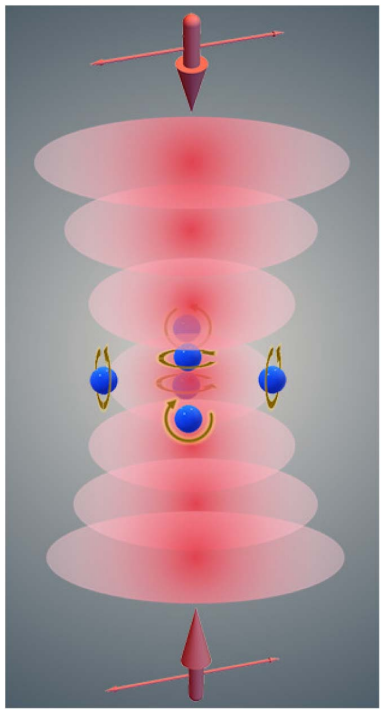

Fig. 1. Schematic of 3D spinning of chiral spheres in a standing wave. This rotation is caused by the intensity-gradient torque, analogous to 3D trapping via gradient forces.

their field-related properties, in the spirit of the classification of optical forces.

2. RESULTS AND DISCUSSION

We start by considering a simple inhomogeneous field consisting of two counterpropagating plane waves polarized along z direction, as depicted in Fig. 2(a). The electric and magnetic vectors of illumination are given by

$$\mathbf{E} = -2E_0 \cos(kx)\hat{\mathbf{z}}, \quad \mathbf{B} = 2\frac{E_0}{c} \sin(kx)\hat{\mathbf{y}}. \tag{1}$$

This standing wave is incident on a sphere made of bi-isotropic chiral material described by the constitutive relation [26]:

$$\begin{aligned} \mathbf{D} &= \varepsilon_0\varepsilon_s\mathbf{E} + i\kappa\sqrt{\varepsilon_0\mu_0}\mathbf{H}, \\ \mathbf{B} &= \mu_0\mu_s\mathbf{H} - i\kappa\sqrt{\varepsilon_0\mu_0}\mathbf{E}, \end{aligned} \tag{2}$$

where the parameter κ describes the particle chirality, and ε_0 (μ_0) and ε_s (μ_s) denote the vacuum and relative permittivity (permeability), respectively.

In this condition, one might not expect the appearance of a torque because the illumination is linearly polarized, carrying no spin angular momentum, and the field momentum is completely canceled by the counterpropagating configuration over the whole space. However, our calculations based on the Lorenz–Mie method show that the particle will experience a torque in the x direction. Also, this torque holds a spatial characteristic consistent with that of the intensity gradient, $\nabla|\mathbf{E}|^2 \propto \sin(2kx)$, which reaches zero at the field nodes and antinodes ($kx = n\pi/2$ for integer n).

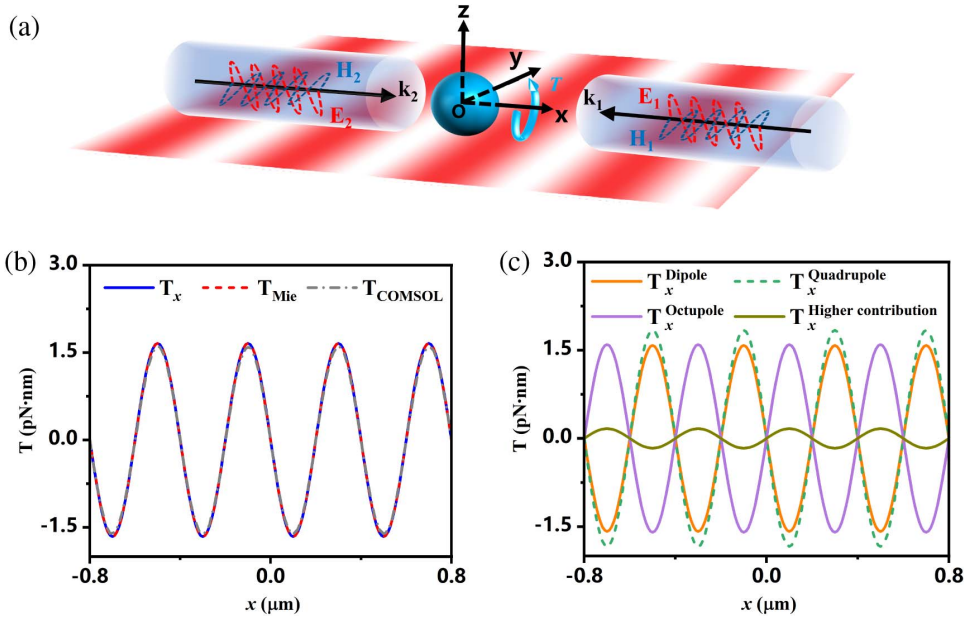

Fig. 2. (a) Schematic illustration of a chiral sphere illuminated by a standing wave composed of two plane waves, with linear polarization and propagating in opposite directions. The electric field is polarized parallel to the z-axis, and the wave vectors $\mathbf{k}_{1,2}$ lie on the xoy plane. The intensity distribution of the interference field is demonstrated by the red and white stripes. The electric intensity gradient is proportional to its magnetic counterpart with a negative scale coefficient. (b) Time-averaged optical torque and (c) its multipolar contributions as a function of the particle's position in the Cartesian coordinate system. The particle parameters satisfy $\varepsilon_s = 2.5 + 0.01i$, $\mu_s = 1$, $\kappa = 0.3$, $r_s = 0.5$ μm, and the incident wavelength is $\lambda = 1.064$ μm.

To reveal the origin of this torque, we resort to the Cartesian multipole expansion model outlined in Ref. [8] and express the torque in terms of the incident field defined by Eq. (1) and the particle's material properties, by which we arrive at (details in Appendix A)

$$\mathbf{T} = \sum_{l=1}^{N} \beta^{(l)} \Re[\gamma_{\mathrm{elec}}^{(l)} \gamma_{x}^{(l)*} - \gamma_{\mathrm{mag}}^{(l)} \gamma_{x}^{(l)*}] \nabla |\mathbf{E}|^2,$$

$$\beta^{(l)} = -\frac{1}{32\pi} \frac{(-2)^l (l+1)^2 (l-1)!}{l^2 (2l-1)!(2l+1)!!}, \tag{3}$$

where $\gamma_x^{(l)}$, $\gamma_{\mathrm{elec}}^{(l)}$ ($\gamma_{\mathrm{mag}}^{(l)}$) represent the polarizabilities due to chiral magnetoelectric coupling and conventional electric (magnetic) responses, respectively. The result obtained from this analytical expression [see the blue line in Fig. 2(b)] agrees with the outcomes from the Lorenz–Mie ($\mathbf{T}_{\mathrm{Mie}}$) and finite element methods ($\mathbf{T}_{\mathrm{COMSOL}}$).

Equation (3) explicitly shows that the torque originates exclusively from the intensity gradient of illumination. The standing wave, thus, serves as an ideal platform to experimentally observe such an intriguing phenomenon. We remark that Eq. (3) is derived from the recoil part of the total torque with the vanishing interception part [8]. It follows that the torque is associated with the interplay of multipoles excited in the particle, as reflected by the product terms of polarizabilities in Eq. (3). Further calculations show that the torque on this particle is dominated by the dipole, quadrupole, and octupole responses, while higher-order contributions are negligible. Notably, each multipole contribution includes only self-interaction terms and excludes any coupling between different orders.

We also notice in Eq. (3) that the intensity-gradient torque exhibits an anti-symmetry concerning the exchange of the electric and magnetic polarizabilities: $\gamma_{\mathrm{elec}}^{(l)} \rightleftarrows \gamma_{\mathrm{mag}}^{(l)}$. This property is clearly shown in Fig. 3, in which the torque is plotted versus the real parts of the particle's relative permittivity $\mathrm{Re}(\varepsilon_s)$ and permeability $\mathrm{Re}(\mu_s)$, with $\Im(\varepsilon_s) = \Im(\mu_s) = 0.01$ and the particle placed at (0.3,0,0) μm; other parameters are consistent with those in Fig. 2(b). Note that ε_s and μ_s are linked to the polarizabilities by the same function according to the Mie theory: $\gamma_{\mathrm{elec}}^{(l)} = F(\varepsilon_s, \sqrt{\varepsilon_s \mu_s})$ and $\gamma_{\mathrm{mag}}^{(l)} = F(\mu_s, \sqrt{\varepsilon_s \mu_s})$ so that the exchange $\varepsilon_s \rightleftarrows \mu_s$ gives rise to $\gamma_{\mathrm{elec}}^{(l)} \rightleftarrows \gamma_{\mathrm{mag}}^{(l)}$. As expected, the result is anti-asymmetric with respect to the black line of $\mu_s = \varepsilon_s$, where the torque vanishes. Therefore, the generation of the intensity-gradient torque entails the breaking of electric-magnetic response symmetry (EMRS): $\gamma_{\mathrm{elec}}^{(l)} \neq \gamma_{\mathrm{mag}}^{(l)}$ or $\varepsilon_s \neq \mu_s$. In this regard, this torque resembles the IPM force, for which the breaking of EMRS is also required [9,27].

Figure 4 emphasizes the chiral nature of the intensity-gradient torque. Specifically, changing the sign of the particle's chiral parameter κ leads to a direction reversal of the torque experienced by the particle so that the torque vanishes for an achiral particle ($\kappa = 0$). This chirality-dependent property is explained by the polarizability $\gamma_x^{(l)}$ in Eq. (3), which is an odd function of the chiral parameter: $\gamma_x^{(l)}(\kappa) = -\gamma_x^{(l)}(-\kappa)$, irrespective of particle size [28]. Interestingly, even with a fixed sign of the chiral parameter κ, the intensity-gradient torque can reverse as the particle size increases. This is because higher-order multipoles become more significant with larger particles, and their relative contributions can cause the total torque to change sign. It is noteworthy that the results depicted in Fig. 4 encompass particle diameters ranging from 0.4λ to 4λ, substantiating the universality of the analytical formulas [Eq. (3)] concerning particle size.

To show the intensity-gradient torque in an experimentally accessible configuration [29,30], calculations were performed using focused Gaussian beams (Fig. 5). In this case, the particle can be stably trapped on-axis by the transverse optical forces. Specifically, the trapping position in the *xoy* plane is determined by the intensity distribution of the interference field, as shown in Fig. 5(a), where the particle is trapped in the region of extreme intensity (or bright region). In the *yoz* plane, there is only one equilibrium position at the center of the beams, as shown

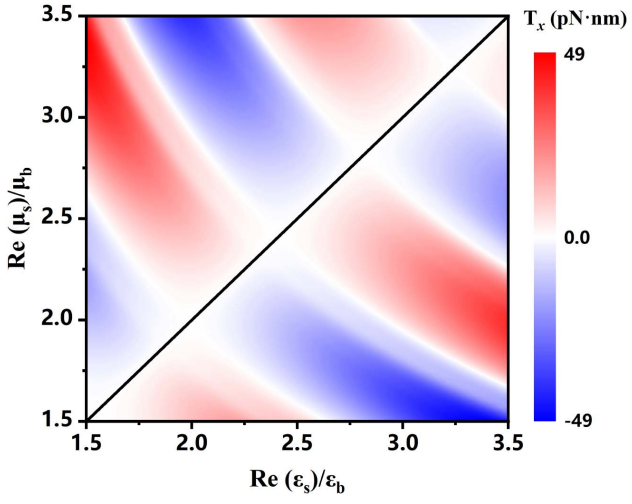

Fig. 3. The optical intensity-gradient torque versus the real parts of the particle's permittivity $\Re(\varepsilon_s)/\varepsilon_b$ and permeability $\Re(\mu_s)/\mu_b$ when a particle is immersed in water (with $\varepsilon_b = 1.33^2$). Their imaginary parts are fixed at $\Im(\varepsilon_s) = \Im(\mu_s) = 0.01$.

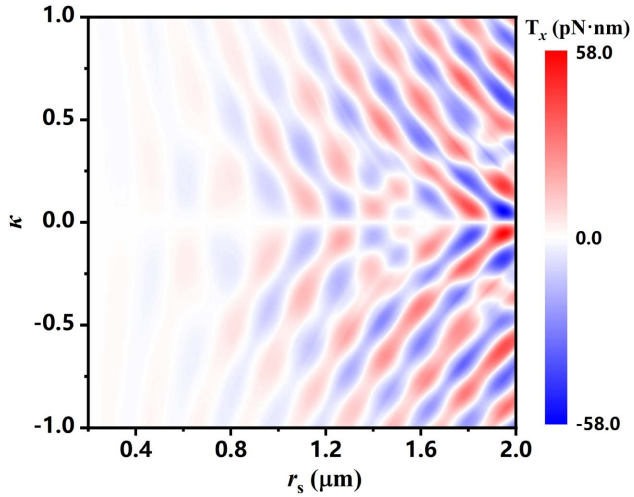

Fig. 4. The spatial profiles of the torque versus the chiral parameter κ and radius r_s. The particle is placed at (0.3,0,0) μm in water, and other parameters are consistent with Fig. 2(b).

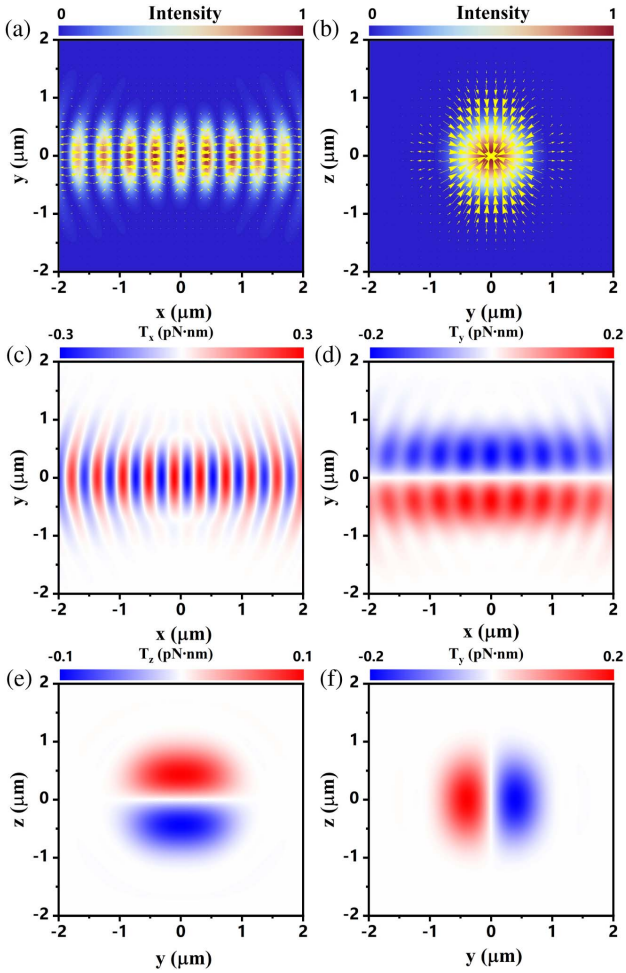

Fig. 5. Simulated 3D rotation in water using intensity-gradient torque, where a chiral Si particle is illuminated by two counterpropagating Gaussian beams along the x-axis, with optical axes lying in the $z = 0$ plane and electric field polarization aligned parallel to the z-axis. The numerical aperture and incident wavelength of each Gaussian beam are 0.7 and 1.064 μm, respectively, and the intensity at beam center is taken as 1 mW/μm^2. The parameters of the Si nanoparticle probe are as follows: $\epsilon_s = 12.1 + 0.2i$, $\mu_s = 1$, $\kappa = 0.5$, and $r_s = 0.5$ μm. Transverse optical forces versus the particle position in the transverse xoy plane (a) and the yoz plane (b). The yellow arrows indicate the magnitude and direction of the transverse forces. The intensity profiles are normalized to their maximum value and presented as the background. Calculated intensity-gradient torques in the x-component (c) and y-component (d) when the particle is located in the xoy plane, as well as in the z-component (e) and y-component (f) when it is placed in the yoz plane.

in Fig. 5(b). Figures 5(c)–5(f) illustrate the three coordinate components of the intensity-gradient torque, calculated using the prevailing Lorenz–Mie method, for a chiral Si nanoparticle probe. Guided by Figs. 5(a) and 5(b), it is clear that the particle does not rotate at the equilibrium point, where the torque vanishes. However, when the particle is slightly displaced from the equilibrium position along any coordinate component, it experiences the intensity-gradient torque in that direction. We emphasize that this torque is unique to chiral particles, so it will not arise for achiral particles used in previous experiments [29]. The sign of the intensity-gradient torque is sensitive to orientation, as the intensity gradient changes direction across space, which results from rapid changes in the intensity of the light field. Therefore, the intensity-gradient torque provides an effective means for 3D rotational control in optical manipulation, enabling the realization of different rotation modes through the adjustment of the intensity distribution. Furthermore, the intensity-gradient torque can be used to control 3D rotation of particles for 3D imaging. In aqueous environments, applying a viscous force can displace the particle from the focus center along a specific direction, thereby enabling directional control of the torque or rotation. This enables the acquisition of 2D projection images from multiple viewing angles, facilitating the development of 3D microscopy techniques [31] such as optical diffraction tomography [32].

The above results have exemplified the existence of the intensity-gradient torque in the special case of standing waves. To generalize this concept, we then assume a generic illumination and incorporate the angular spectrum theory [9] into the Cartesian multipole expansion method [8]. After a lengthy algebra, we decompose the total torque into two parts:

$$\mathbf{T} = \sum_{l=1}^{N} \mathbf{T}^{(l)}_{\text{achiral}} + \sum_{l=1}^{N} \mathbf{T}^{(l)}_{\text{chiral}}, \tag{4}$$

where $\mathbf{T}^{(l)}_{\text{achiral}}$ and $\mathbf{T}^{(l)}_{\text{chiral}}$ represent the 2^l-pole contributions independent and dependent of the particle chirality, respectively. The former was shown associated to the optical spin, the momentum curl, and the gradient of reactive helicity [33] of illumination in a recent work [34]. We find that it is constructive to categorize the l-order chiral torque into six components according to the field-related quantities:

$$\mathbf{T}^{(l)}_{\text{chiral}} = \mathbf{T}^{(l)}_{\text{spin}} + \mathbf{T}^{(l)}_{\text{curl}} + \mathbf{T}^{(l)}_{\text{IG}} + \mathbf{T}^{(l)}_{\text{PG}} + \mathbf{T}^{(l)}_{\text{PM}} + \mathbf{T}^{(l)}_{\text{IPM}}, \tag{5}$$

with

$$\begin{aligned}
\mathbf{T}^{(l)}_{\text{spin}} &= \hat{\mathcal{C}}^{(l)}_{\text{spin}}[\mathfrak{F}(\mathbf{E}^* \times \mathbf{E}) + c^2\mathfrak{F}(\mathbf{B}^* \times \mathbf{B})],\\
\mathbf{T}^{(l)}_{\text{curl}} &= \hat{\mathcal{C}}^{(l)}_{\text{curl}} \nabla \times \mathfrak{R}(\mathbf{E}^* \times \mathbf{B}),\\
\mathbf{T}^{(l)}_{\text{IG}} &= \hat{\mathcal{C}}^{(l)}_{\text{IG}}(\nabla|\mathbf{E}|^2 - c^2\nabla|\mathbf{B}|^2),\\
\mathbf{T}^{(l)}_{\text{PG}} &= \hat{\mathcal{C}}^{(l)}_{\text{PG}}[\mathfrak{F}(\nabla\mathbf{E} \cdot \mathbf{E}^*) + c^2\mathfrak{F}(\nabla\mathbf{B} \cdot \mathbf{B}^*)],\\
\mathbf{T}^{(l)}_{\text{PM}} &= \hat{\mathcal{C}}^{(l)}_{\text{PM}}\mathfrak{R}(\mathbf{E}^* \times \mathbf{B}),\\
\mathbf{T}^{(l)}_{\text{IPM}} &= \hat{\mathcal{C}}^{(l)}_{\text{IPM}}\mathfrak{F}(\mathbf{E}^* \times \mathbf{B}),
\end{aligned} \tag{6}$$

where the prefactors are determined by the material properties of the particle (details in Appendix B). The first two terms, $\mathbf{T}^{(l)}_{\text{spin}}$ and $\mathbf{T}^{(l)}_{\text{curl}}$, indicate that the optical spin and momentum curl account for the chiral torque, in addition to the achiral one [34]. It is interesting to note that the optical spin is coupled to the chiral torque by its dual-symmetric form [35,36], $\mathfrak{F}(\mathbf{E}^* \times \mathbf{E}) + c^2\mathfrak{F}(\mathbf{B}^* \times \mathbf{B})$, but the electric and magnetic spins contribute differently to the achiral torque in general [15].

The field quantities arising in the last four components are unavailable to the achiral torque [34], but they are responsible for the well-known intensity-gradient force [7,11], phase-gradient force [12], radiation pressure, and IPM force on achiral particles [7,9,13]. In this connection, $\mathbf{T}^{(l)}_{\text{IG}}$, $\mathbf{T}^{(l)}_{\text{PG}}$, $\mathbf{T}^{(l)}_{\text{PM}}$, and $\mathbf{T}^{(l)}_{\text{IPM}}$

Table 1. A List of Optical Force/Torque Counterparts, Highlighting Their Relevance to Light Structure and Generation Requirements on Material Properties

		Material Properties (Force/Torque)			
Force/Torque Category	Light Structure	Chirality	EMRS Breaking	High-Order Multipoles	Multipole Interplay
Intensity gradient	$\nabla\lvert\mathbf{E}\rvert^2$ or $\nabla\lvert\mathbf{H}\rvert^2$	No/Yes	No/Yes	No/Yes	No/Yes
Phase gradient	$\mathfrak{I}[\mathbf{E}^*\cdot(\nabla\mathbf{E})]$ or $\mathfrak{I}[\mathbf{H}^*\cdot(\nabla\mathbf{H})]$	No/Yes	No/No	No/Yes	No/No
Kinetic momentum	$\mathfrak{R}(\mathbf{E}^*\times\mathbf{H})$	No/Yes	No/No	No/No	Yes/No
Reactive momentum	$\mathfrak{I}(\mathbf{E}^*\times\mathbf{H})$	No/Yes	Yes/Yes	No/No	Yes/Yes
Spin	$\mathfrak{I}(\mathbf{E}^*\times\mathbf{E})$ or $\mathfrak{I}(\mathbf{H}^*\times\mathbf{H})$	Yes/No	No/No	No/No	No/No
Reactive helicity gradient	$\nabla\mathfrak{R}(\mathbf{E}^*\cdot\mathbf{H})$	Yes/No	Yes/Yes	Yes/Yes	Yes/No
Momentum curl	$\nabla\times\mathfrak{R}(\mathbf{E}^*\times\mathbf{H})$	Yes/No	No/No	No/Yes	No/No

represent the angular analogs of these types of force. It is worth noting that the standard momentum, $\mathfrak{R}(\mathbf{E}^*\times\mathbf{H})$, is sometimes written as the sum of its spin and orbital parts, especially in literature focusing on the optical force due to Belinfante's spin momentum (BSM) [37–40]. One may also perform the spin–orbit decomposition for the momentum in $\mathbf{T}_{\mathrm{PM}}^{(l)}$ so that the BSM can manifest itself as the torque, but we would keep its original form for the mathematical elegance of our theory. We stress that the IPM torque $\mathbf{T}_{\mathrm{IPM}}^{(l)}$, akin to the IPM force [7,9], can act on a dipole particle for a generic field, whereas the intensity-gradient torque, $\mathbf{T}_{\mathrm{IG}}^{(l)}$, requires the excitation of high-order ($l>1$) multipoles, as $\hat{C}_{\mathrm{IG}}^{(l)}=0$ for $l=1$. However, in some special fields [e.g., the standing wave shown in Fig. 2(a)], the reactive momentum, $\mathfrak{I}(\mathbf{E}^*\times\mathbf{B})$, may reduce to its orbital part [33,41] (which is proportional to $\nabla\lvert\mathbf{E}\rvert^2-c^2\nabla\lvert\mathbf{B}\rvert^2$), such that the intensity gradient induces the torque via the dipole response [Fig. 2(c)].

To gain an overview of the principle of optical force and torque, Table 1 compares the torques with their force counterparts [7,9,26,42,43] featuring the same light structure in arbitrary monochromatic optical fields, in terms of the generation requirements on material properties. It is of marked interest that each type of optical force (or torque) for an achiral particle finds its analog in the torque (or force) on a chiral one. The breaking of EMRS [27] is necessary for the intensity-gradient torque and all mechanical effects induced by reactive quantities. High-order multipole excitation is a requisite for torques, except for the conventional spin torque and those due to the field momenta including kinetic and reactive. Also, the mechanical manifestations of some field quantities (e.g., the IPM force and the intensity-gradient torque) must rely on the multipole interplay, which highlights their recoil nature. At last, we remark that the gradient of standard helicity (not listed in the table), $\nabla\mathfrak{I}(\mathbf{E}^*\cdot\mathbf{H})$, may also contribute to the optical force for chiral particles [26,43] but is shown irrelevant to the torque in light of our theory.

3. CONCLUSION

In summary, we have discovered the intensity-gradient torque by exploiting the interplay of chiral multipoles and have built a generic multipole model, which expands the classifying framework of optical torques from nonchiral [34] to chiral. The intensity-gradient torque offers unique opportunities for particle spinning in terms of frequency and degree of freedom, in that the intensity inhomogeneity may be significant with a small power density [11] and in that the distribution of optical intensity, in practice, is easier to customize than phase and polarization. It also opens new possibilities for near-field tweezers [44,45], in which the field localized beyond the diffraction limit is expected to enhance strongly the torque. In fact, the intensity gradient and spin are compatible properties of light, which promises their integration into chiral and rotational optomechanics.

As a closing remark, we would point out that material nonreciprocity and anisotropy, which are beyond the scope of this paper, also play an important role in light–matter interaction. Although this subject has recently been actively researched experimentally and numerically in optical manipulations [23,46–52], its theory is yet to be well developed, especially in scenarios of high-order multipoles. We anticipate that our multipole framework, which is established from the fundamental constitutive relation and first principles, will set methodologically in the framework of classical electromagnetic theory an inspiring example for the development of optical force and torque theories for non-reciprocal and anisotropic particles.

APPENDIX A: OPTICAL INTENSITY-GRADIENT TORQUE IN STANDING WAVE FIELD

The period-averaged optical torques $\langle\mathbf{T}\rangle$ on a particle in generic monochromatic optical fields are written as a sum of recoil torques $\langle\mathbf{T}_{\mathrm{rec}}\rangle$ and interception torques $\langle\mathbf{T}_{\mathrm{int}}\rangle$, which read, respectively [8],

$$\langle\mathbf{T}\rangle=\langle\mathbf{T}_{\mathrm{rec}}\rangle+\langle\mathbf{T}_{\mathrm{int}}\rangle,\quad \langle\mathbf{T}_{\mathrm{rec}}\rangle=\sum_{l=1}^{\infty}\langle\mathbf{T}_{\mathrm{rec}}^{(l)}\rangle,$$
$$\langle\mathbf{T}_{\mathrm{int}}\rangle=\sum_{l=1}^{\infty}\langle\mathbf{T}_{\mathrm{int}}^{(l)}\rangle, \tag{A1}$$

$$\langle\mathbf{T}_{\mathrm{rec}}^{(l)}\rangle=-\frac{1}{8\pi\varepsilon_0}\sum_{l=1}^{\infty}\frac{2^l(l+1)k^{2l+1}}{(2l+1)!}\times\mathfrak{I}\Big[\overleftrightarrow{\mathbb{O}}_{\mathrm{elec}}^{(l)}\overset{(l-1)}{\cdot\cdot}\overleftrightarrow{\mathbb{O}}_{\mathrm{elec}}^{(l)*}+\frac{1}{c^2}\overleftrightarrow{\mathbb{O}}_{\mathrm{mag}}^{(l)}\overset{(l-1)}{\cdot\cdot}\overleftrightarrow{\mathbb{O}}_{\mathrm{mag}}^{(l)*}\Big]\overset{(2)}{\cdot\cdot}\overleftrightarrow{\epsilon}, \tag{A2}$$

$$\begin{aligned}\langle \mathbf{T}_{\mathrm{int}}^{(l)}\rangle = & \frac{l-1}{2l!}\mathfrak{R}[(\nabla^{(l-1)}\mathbf{E}^*)\overset{(l-1)}{\cdot\cdot}\overset{\leftrightarrow}{\mathbb{O}}{}^{(l)}_{\mathrm{elec}} \\ & + (\nabla^{(l-1)}\mathbf{B}^*)\overset{(l-1)}{\cdot\cdot}\overset{\leftrightarrow}{\mathbb{O}}{}^{(l)}_{\mathrm{mag}}]\overset{(2)}{\cdot\cdot}\overset{\leftrightarrow}{\epsilon} \\ & - \frac{1}{2l!}\mathfrak{R}[\overset{\leftrightarrow}{\mathbb{O}}{}^{(l)}_{\mathrm{elec}}\overset{(l-1)}{\cdot\cdot}(\nabla^{(l-1)}\mathbf{E}^*) \\ & + \overset{\leftrightarrow}{\mathbb{O}}{}^{(l)}_{\mathrm{mag}}\overset{(l-1)}{\cdot\cdot}(\nabla^{(l-1)}\mathbf{B}^*)]\overset{(2)}{\cdot\cdot}\overset{\leftrightarrow}{\epsilon}, \end{aligned} \tag{A3}$$

with $\overset{\leftrightarrow}{\epsilon}$ denoting the Levi–Civita anti-symmetric tensor and the superscript * designating the complex conjugate. $\mathfrak{F}$ and $\mathfrak{R}$ denote extracting the imaginary and real components. $\mathbf{E}$ ($\mathbf{B}$) denote the electric (magnetic) fields in which the particle is immersed. The multiple contraction $\overset{(m)}{\cdot\cdot}$ operating on two tensors with ranks l and l' obtains a tensor of rank $1+l'-2m$ defined by

$$\begin{aligned}&\overset{\leftrightarrow}{\mathbb{A}}{}^{(l)}\overset{(m)}{\cdot\cdot}\overset{\leftrightarrow}{\mathbb{B}}{}^{(l')} = \mathbb{A}^{(l)}_{i_1 i_2\cdots i_{l-m}k_1k_2\cdots k_m}\mathbb{B}^{(l')}_{k_m\cdots k_2k_1j_{m+1}j_{m+2}\cdots j_{l'}}, \\ &0\le m\le \min[l,l'],\end{aligned}$$

where it is assumed that the repeated indices are summed, i.e., the tensor contraction is consecutive on the two nearest indices of the two index sequences. The total symmetric and traceless [53] tensors $\overset{\leftrightarrow}{\mathbb{O}}{}^{(l)}_{\mathrm{elec(mag)}}$ denote the electric (magnetic) 2^l-pole moments excited on a chiral particle,

$$\overset{\leftrightarrow}{\mathbb{O}}{}^{(l)}_{\mathrm{elec(mag)}} = \gamma^{(l)}_{\mathrm{elec(mag)}}\overset{\leftrightarrow}{\mathbb{L}}{}^{(l)}_{\mathrm{elec(mag)}} \pm \gamma^{(l)}_{x}\overset{\leftrightarrow}{\mathbb{L}}{}^{(l)}_{\mathrm{mag(elec)}}. \tag{A4}$$

The positive and negative signs before $\gamma^{(l)}_x$ correspond to electric and magnetic 2^l-pole moments, $\overset{\leftrightarrow}{\mathbb{O}}{}^{(l)}_{\mathrm{elec}}$ and $\overset{\leftrightarrow}{\mathbb{O}}{}^{(l)}_{\mathrm{mag}}$, respectively. $\gamma^{(l)}_x$, $\gamma^{(l)}_{\mathrm{elec}}$, and $\gamma^{(l)}_{\mathrm{mag}}$ are the polarizabilities due to chiral magnetoelectric coupling, normal electric and magnetic responses, reading as

$$\begin{aligned}&\gamma^{(l)}_{\mathrm{elec}} = \frac{i\zeta_l a_l}{k^{2l+1}}, \quad \gamma^{(l)}_{\mathrm{mag}} = \frac{ic^2\zeta_l b_l}{k^{2l+1}}, \quad \gamma^{(l)}_{x} = -\frac{c\zeta_l c_l}{k^{2l+1}}, \\ &\text{with} \quad \zeta_l = \frac{4\pi\varepsilon_0 l(2l+1)!!}{(l+1)},\end{aligned} \tag{A5}$$

where i denotes the imaginary unit and c is the speed of light in the ambient medium. The multipole moment given by Eq. (A4) degenerates to achiral particles, when the Mie coefficient c_l indicating chiral magnetoelectric coupling is set to 0. The tensors $\mathbb{L}^{(l)}_{\mathrm{elec}}$ and $\mathbb{L}^{(l)}_{\mathrm{mag}}$ describe the incident field characteristic,

$$\begin{aligned}&\overset{\leftrightarrow}{\mathbb{L}}{}^{(l)}_{\mathrm{elec\ (mag)}} = \sum_{m=0}^{\lfloor\frac{l-1}{2}\rfloor} d_{l,m}k^{2m}\overset{\leftrightarrow}{\mathbb{N}}{}^{(l,m)}_{\mathrm{elec\ (mag)}}, \\ &d_{l,m} = \frac{1}{4^m}\frac{l!}{m!}\frac{\Gamma\left(l-m+\frac{1}{2}\right)}{\Gamma\left(l+\frac{1}{2}\right)\Gamma(l-2m)}\frac{1}{l}, \quad \text{with } d_{l,0}=1,\end{aligned} \tag{A6}$$

where the totally traceless and symmetric rank-l tensors are

$$\begin{aligned}&\overset{\leftrightarrow}{\mathbb{N}}{}^{(l,\mathrm{m})}_{\mathrm{elec(mag)}} = \hat{\mathcal{S}}\left[\overbrace{\overset{\leftrightarrow}{\mathbb{I}}\otimes\overset{\leftrightarrow}{\mathbb{I}}\otimes\cdots\overset{\leftrightarrow}{\mathbb{I}}}^{m}\otimes\overset{\leftrightarrow}{\mathbb{M}}{}^{(l-2m)}_{\mathrm{elec(mag)}}\right] \\ &\text{with } \overset{\leftrightarrow}{\mathbb{N}}{}^{(l,0)}_{\mathrm{elec(mag)}} \equiv \overset{\leftrightarrow}{\mathbb{M}}{}^{(l)}_{\mathrm{elec(mag)}}.\end{aligned} \tag{A7}$$

Here, $\overset{\leftrightarrow}{\mathbb{I}}$ and $\otimes$ denote the unit dyad of dimension 3 and the tensor product, respectively, while $\hat{\mathcal{S}}$ denotes the symmetry operator. $\overset{\leftrightarrow}{\mathbb{M}}{}^{(n)}_{\mathrm{elec(mag)}}$ represents completely symmetric tensors describing the symmetric multiple gradients of the incident field, which is denoted by

$$\begin{aligned}\overset{\leftrightarrow}{\mathbb{M}}{}^{(n)}_{\mathrm{elec}} &= \hat{\mathcal{S}}[\nabla^{(n-1)}\mathbf{E}] = \hat{\mathcal{S}}[\overbrace{\nabla\nabla\cdots\nabla}^{n-1}\mathbf{E}] \\ &= \frac{1}{n}\sum_{j=1}^{n}\partial_{i_1}\cdots\partial_{i_{j-1}}\partial_{i_n}\partial_{i_{j+1}}\cdots\partial_{i_{n-1}}\mathbf{E}_{i_j}, \\ \overset{\leftrightarrow}{\mathbb{M}}{}^{(n)}_{\mathrm{mag}} &= \hat{\mathcal{S}}[\nabla^{(n-1)}\mathbf{B}] = \hat{\mathcal{S}}[\overbrace{\nabla\nabla\cdots\nabla}^{n-1}\mathbf{B}] \\ &= \frac{1}{n}\sum_{j=1}^{n}\partial_{i_1}\cdots\partial_{i_{j-1}}\partial_{i_n}\partial_{i_{j+1}}\cdots\partial_{i_{n-1}}\mathbf{B}_{i_j}.\end{aligned} \tag{A8}$$

In above equation, $\nabla^{(n)}$ denotes that the n-fold gradient is taken continuously, and $\mathbf{E}_j$ ($\mathbf{B}_j$) is the jth Cartesian component of the electric (magnetic) field.

Due to the explicit mathematical relations for electric and magnetic multipoles in spherical particles as presented in Eq. (A4), it becomes possible to derive an analytical expression for the optical torque acting upon an isotropic chiral spherical particle. This expression can be represented in an explicit mathematical form that involves the product of polarizability and field quantities,

$$\langle \mathbf{T}^{e(l)}_{\mathrm{rec}}\rangle = -\frac{2^l(l+1)k^{2l+1}}{8\pi(2l+1)!}\sum_{m=0}^{\lfloor\frac{l-1}{2}\rfloor}k^{4m}h_{l,m}\mathfrak{F}\left[\left(\eta^{(l)}_{\mathrm{hhc}}+\eta^{(l)}_{\mathrm{eec}}\right)\boldsymbol{\tau}^{(l-2m)}_{\mathrm{exe}}\right], \tag{A9}$$

$$\langle \mathbf{T}^{m(l)}_{\mathrm{rec}}\rangle = -\frac{2^l(l+1)k^{2l+1}}{8\pi(2l+1)!}\sum_{m=0}^{\lfloor\frac{l-1}{2}\rfloor}k^{4m}h_{l,m}\mathfrak{F}\left[\left(\eta^{(l)}_{\mathrm{mmc}}+\eta^{(l)}_{\mathrm{hhc}}\right)\boldsymbol{\tau}^{(l-2m)}_{\mathrm{mxm}}\right], \tag{A10}$$

$$\begin{aligned}\langle \mathbf{T}^{\varkappa(l)}_{\mathrm{rec}}\rangle = & -\frac{2^l(l+1)k^{2l+1}}{8\pi(2l+1)!}\sum_{m=0}^{\lfloor\frac{l-1}{2}\rfloor}k^{4m}h_{l,m} \\ & \times\mathfrak{F}\left[\left(\eta^{(l)}_{\mathrm{ehc}}-\eta^{(l)*}_{\mathrm{mhc}}\right)\boldsymbol{\tau}^{(l-2m)}_{\mathrm{exmc}}+\left(\eta^{(l)*}_{\mathrm{ehc}}-\eta^{(l)}_{\mathrm{mhc}}\right)\boldsymbol{\tau}^{(l-2m)}_{\mathrm{mxec}}\right],\end{aligned} \tag{A11}$$

$$\langle \mathbf{T}^{e(l)}_{\mathrm{int}}\rangle = -\frac{1}{2(l-1)!}\sum_{m=0}^{\lfloor\frac{l-1}{2}\rfloor}k^{4m}h_{l,m}\mathfrak{R}\left[\gamma^{(l)}_{\mathrm{elec}}\boldsymbol{\tau}^{(l-2m)}_{\mathrm{exe}}\right], \tag{A12}$$

$$\langle \mathbf{T}_{\rm int}^{m(l)} \rangle = -\frac{1}{2(l-1)!}\sum_{m=0}^{\lfloor \frac{l-1}{2} \rfloor} k^{4m} h_{l,m} \Re\left[\gamma_{\rm mag}^{(l)} \boldsymbol{\tau}_{\rm mxm}^{(l-2m)}\right], \quad \text{(A13)}$$

$$\langle \mathbf{T}_{\rm int}^{x(l)} \rangle = -\frac{1}{2(l-1)!}\sum_{m=0}^{\lfloor \frac{l-1}{2} \rfloor} k^{4m} h_{l,m} \Re\left[\gamma_{x}^{(l)} \left(\boldsymbol{\tau}_{\rm mxec}^{(l-2m)} - \boldsymbol{\tau}_{\rm exmc}^{(l-2m)}\right)\right], \quad \text{(A14)}$$

where the products of polarizabilities η are given by

$$\eta_{\rm eec}^{(l)} = \gamma_{\rm elec}^{(l)} \gamma_{\rm elec}^{(l)*}, \quad \eta_{\rm mmc}^{(l)} = \gamma_{\rm mag}^{(l)} \gamma_{\rm mag}^{(l)*}, \quad \eta_{\rm hhc}^{(l)} = \gamma_{x}^{(l)} \gamma_{x}^{(l)*},$$
$$\eta_{\rm ehc}^{(l)} = \gamma_{\rm elec}^{(l)} \gamma_{x}^{(l)*}, \quad \eta_{\rm mhc}^{(l)} = \gamma_{\rm mag}^{(l)} \gamma_{x}^{(l)*}. \quad \text{(A15)}$$

In deriving Eqs. (A9)–(A14), the following relations were used:

$$\left[\overleftrightarrow{\mathbb{L}}_{\rm elec}^{(l)} \overset{(l-1)}{\cdot\cdot} \overleftrightarrow{\mathbb{L}}_{\rm elec}^{(l)*}\right] \overset{(2)}{\cdot\cdot} \overleftrightarrow{\epsilon} = \sum_{m=0}^{\lfloor \frac{l-1}{2} \rfloor} k^{4m} h_{l,m} \boldsymbol{\tau}_{\rm exe}^{(l-2m)},$$
$$\left[\overleftrightarrow{\mathbb{L}}_{\rm mag}^{(l)} \overset{(l-1)}{\cdot\cdot} \overleftrightarrow{\mathbb{L}}_{\rm mag}^{(l)*}\right] \overset{(l-1)}{\cdot\cdot} \overleftrightarrow{\epsilon} = \sum_{m=0}^{\lfloor \frac{l-1}{2} \rfloor} k^{4m} h_{l,m} \boldsymbol{\tau}_{\rm mxm}^{(l-2m)},$$
$$\left[\overleftrightarrow{\mathbb{L}}_{\rm elec}^{(l)} \overset{(l-1)}{\cdot\cdot} \overleftrightarrow{\mathbb{L}}_{\rm mag}^{(l)*}\right] \overset{(2)}{\cdot\cdot} \overleftrightarrow{\epsilon} = \sum_{m=0}^{\lfloor \frac{l-1}{2} \rfloor} k^{4m} h_{l,m} \boldsymbol{\tau}_{\rm exmc}^{(l-2m)},$$
$$\left[\overleftrightarrow{\mathbb{L}}_{\rm mag}^{(l)} \overset{(l-1)}{\cdot\cdot} \overleftrightarrow{\mathbb{L}}_{\rm elec}^{(l)*}\right] \overset{(2)}{\cdot\cdot} \overleftrightarrow{\epsilon} = \sum_{m=0}^{\lfloor \frac{l-1}{2} \rfloor} k^{4m} h_{l,m} \boldsymbol{\tau}_{\rm mxec}^{(l-2m)}, \quad \text{(A16)}$$

with

$$h_{l,m} = \frac{(l-2m)^2}{l^2}(-1)^m d_{l,m},$$
$$\boldsymbol{\tau}_{\rm exe}^{(l-2m)} = [\overleftrightarrow{\mathbb{M}}_{\rm elec}^{(1-2m)} \overset{(1-2m-1)}{\cdot\cdot} \overleftrightarrow{\mathbb{M}}_{\rm elec}^{(1-2m)*}] \overset{(2)}{\cdot\cdot} \overleftrightarrow{\epsilon},$$
$$\boldsymbol{\tau}_{\rm mxm}^{(l-2m)} = [\overleftrightarrow{\mathbb{M}}_{\rm mag}^{(1-2m)} \overset{(1-2m-1)}{\cdot\cdot} \overleftrightarrow{\mathbb{M}}_{\rm mag}^{(1-2m)*}] \overset{(2)}{\cdot\cdot} \overleftrightarrow{\epsilon},$$
$$\boldsymbol{\tau}_{\rm exmc}^{(l-2m)} = [\overleftrightarrow{\mathbb{M}}_{\rm elec}^{(1-2m)} \overset{(1-2m-1)}{\cdot\cdot} \overleftrightarrow{\mathbb{M}}_{\rm mag}^{(1-2m)*}] \overset{(2)}{\cdot\cdot} \overleftrightarrow{\epsilon},$$
$$\boldsymbol{\tau}_{\rm mxec}^{(l-2m)} = [\overleftrightarrow{\mathbb{M}}_{\rm mag}^{(1-2m)} \overset{(1-2m-1)}{\cdot\cdot} \overleftrightarrow{\mathbb{M}}_{\rm elec}^{(1-2m)*}] \overset{(2)}{\cdot\cdot} \overleftrightarrow{\epsilon}. \quad \text{(A17)}$$

Next, we focus on the relationship between optical torques and specific field quantities. A necessary element is to write a generic monochromatic field in a form similar to the angular spectrum representation [8,54],

$$\mathbf{E} = \oint_{4\pi} \boldsymbol{e}_{\boldsymbol{u}} e^{ik\boldsymbol{u}\cdot\boldsymbol{r}} d\Omega_u, \quad \mathbf{H} = \frac{1}{Z_0}\oint_{4\pi} \boldsymbol{h}_{\boldsymbol{u}} e^{ik\boldsymbol{u}\cdot\boldsymbol{r}} d\Omega_u. \quad \text{(A18)}$$

The direction of the wave vector is shown by the real unit vector $\boldsymbol{u}$. The electric and magnetic angular spectra $\boldsymbol{e}_{\boldsymbol{u}}$ and $\boldsymbol{h}_{\boldsymbol{u}}$ depend only on $\boldsymbol{u}$, which are independent of $\boldsymbol{r}$ and satisfy $\boldsymbol{u}\times\boldsymbol{e}_{\boldsymbol{u}} = \boldsymbol{h}_{\boldsymbol{u}}$ and $\boldsymbol{h}_{\boldsymbol{u}}\times\boldsymbol{u} = \boldsymbol{e}_{\boldsymbol{u}}$. The integration is over the unit sphere of $\boldsymbol{u}$.

Certain field moments are defined in the reciprocal space, for integer n, before the derivation that follows:

$$D_{\rm ee}^{(n)} = \left[\nabla^{(n-1)}\mathbf{E}\right] \overset{(n)}{\vdots} \left[\nabla^{(n-1)}\mathbf{E}^*\right]$$
$$= k^{2n-2}\oint_{4\pi} d\Omega_u \oint_{4\pi} d\Omega_v (\boldsymbol{u}\cdot\boldsymbol{v})^{(n-1)} \left(\boldsymbol{e}_{\boldsymbol{u}}\cdot\boldsymbol{e}_{\boldsymbol{v}}^*\right) e^{ik(\boldsymbol{u}-\boldsymbol{v})\cdot\boldsymbol{r}},$$
$$D_{\rm mm}^{(n)} = \left[\nabla^{(n-1)}\mathbf{B}\right] \overset{(n)}{\vdots} \left[\nabla^{(n-1)}\mathbf{B}^*\right]$$
$$= \frac{k^{2n-2}}{c^2}\oint_{4\pi} d\Omega_u \oint_{4\pi} d\Omega_v (\boldsymbol{u}\cdot\boldsymbol{v})^{n-1} \left(\boldsymbol{h}_{\boldsymbol{u}}\cdot\boldsymbol{h}_{\boldsymbol{v}}^*\right) e^{ik(\boldsymbol{u}-\boldsymbol{v})\cdot\boldsymbol{r}},$$
$$D_{\rm em}^{(n)} = \left[\nabla^{(n-1)}\mathbf{E}\right] \overset{(n)}{\vdots} \left[\nabla^{(n-1)}\mathbf{B}^*\right]$$
$$= \frac{k^{2n-2}}{c}\oint_{4\pi} d\Omega_u \oint_{4\pi} d\Omega_v (\boldsymbol{u}\cdot\boldsymbol{v})^{n-1} \left(\boldsymbol{e}_{\boldsymbol{u}}\cdot\boldsymbol{h}_{\boldsymbol{v}}^*\right) e^{ik(\boldsymbol{u}-\boldsymbol{v})\cdot\boldsymbol{r}},$$
$$D_{\rm me}^{(n)} = \left[\nabla^{(n-1)}\mathbf{B}\right] \overset{(n)}{\vdots} \left[\nabla^{(n-1)}\mathbf{E}^*\right] = D_{\rm em}^{(n)*},$$
$$\mathbf{S}_{\rm ee}^{(n)} = \left[\left(\nabla^{(n-1)}\mathbf{E}\right) \overset{(n-1)}{\vdots} \left(\nabla^{(n-1)}\mathbf{E}^*\right)\right] \overset{(2)}{\vdots} \overleftrightarrow{\epsilon}$$
$$= k^{2n-2}\oint_{4\pi} d\Omega_u \oint_{4\pi} d\Omega_v (\boldsymbol{u}\cdot\boldsymbol{v})^{n-1} \left(\boldsymbol{e}_{\boldsymbol{u}}\times\boldsymbol{e}_{\boldsymbol{v}}^*\right) e^{ik(\boldsymbol{u}-\boldsymbol{v})\cdot\boldsymbol{r}},$$
$$\mathbf{S}_{\rm mm}^{(n)} = \left[\left(\nabla^{(n-1)}\mathbf{B}\right) \overset{(n-1)}{\vdots} \left(\nabla^{(n-1)}\mathbf{B}^*\right)\right] \overset{(2)}{\vdots} \overleftrightarrow{\epsilon}$$
$$= \frac{k^{2n-2}}{c^2}\oint_{4\pi} d\Omega_u \oint_{4\pi} d\Omega_v (\boldsymbol{u}\cdot\boldsymbol{v})^{n-1} \left(\boldsymbol{h}_{\boldsymbol{u}}\times\boldsymbol{h}_{\boldsymbol{v}}^*\right) e^{ik(\boldsymbol{u}-\boldsymbol{v})\cdot\boldsymbol{r}},$$
$$\mathbf{S}_{\rm em}^{(n)} = \left[\left(\nabla^{(n-1)}\mathbf{E}\right) \overset{(n-1)}{\vdots} \left(\nabla^{(n-1)}\mathbf{B}^*\right)\right] \overset{(2)}{\vdots} \overleftrightarrow{\epsilon}$$
$$= \frac{k^{2n-2}}{c}\oint_{4\pi} d\Omega_u \oint_{4\pi} d\Omega_v (\boldsymbol{u}\cdot\boldsymbol{v})^{n-1} \left(\boldsymbol{e}_{\boldsymbol{u}}\times\boldsymbol{h}_{\boldsymbol{v}}^*\right) e^{ik(\boldsymbol{u}-\boldsymbol{v})\cdot\boldsymbol{r}},$$
$$\mathbf{S}_{\rm me}^{(n)} = \left[\left(\nabla^{(n-1)}\mathbf{B}\right) \overset{(n-1)}{\vdots} \left(\nabla^{(n-1)}\mathbf{E}^*\right)\right] \overset{(2)}{\vdots} \overleftrightarrow{\epsilon} = -\mathbf{S}_{\rm em}^{(n)*}, \quad \text{(A19)}$$

where we have defined the second kind of multiple tensor contraction, denoted by $\overset{(n)}{\vdots}$,

$$\overleftrightarrow{\mathbb{A}}^{(l)} \overset{(m)}{\vdots} \overleftrightarrow{\mathbb{B}}^{(l')} = \mathbb{A}^{(l)}_{k_1 k_2 \cdots k_m i_{m+1} i_{m+2} \cdots i_l} \mathbb{B}^{(l')}_{k_1 k_2 \cdots k_m j_{m+1} j_{m+2} \cdots j_{l'}},$$
$$0 \le m \le \min[l, l'], \quad \text{(A20)}$$

that is, the tensor contraction is made over the corresponding leftmost indices in the two index sequences.

After a series of tedious but not complicated derivations, the vectors $\boldsymbol{\tau}_{\rm exe}^{(n)}$, $\boldsymbol{\tau}_{\rm mxm}^{(n)}$, $\boldsymbol{\tau}_{\rm exmc}^{(n)}$, and $\tau_{\rm mxec}^{(n)}$, given by Eq. (A17), are rewritten in terms of vectors D and $\mathbf{S}$ defined in Eq. (A19). The final results are shown as follows:

$$\begin{aligned}
\boldsymbol{\tau}_{\mathrm{exe}}^{(n)} &= \frac{ick(n-1)}{n}\left[\mathbf{Z}_{\mathrm{me}}^{(n-1)} + \mathbf{Z}_{\mathrm{me}}^{(n-1)*}\right] \\
&+ \frac{ick^3(n-1)(n-2)}{n^2}\left[\mathbf{Z}_{\mathrm{em}}^{(n-2)} + \mathbf{Z}_{\mathrm{em}}^{(n-2)*}\right] \\
&- \mathbf{S}_{\mathrm{ee}}^{(n)} - \frac{c^2k^2(n-1)}{n^2}\mathbf{S}_{\mathrm{mm}}^{(n-1)} + \frac{k^4(n-1)(n-2)}{n^2}\mathbf{S}_{\mathrm{ee}}^{(n-2)}, \\
\boldsymbol{\tau}_{\mathrm{mxm}}^{(n)} &= -\frac{ik(n-1)}{nc}\left[\mathbf{Z}_{\mathrm{em}}^{(n-1)} + \mathbf{Z}_{\mathrm{em}}^{(n-1)*}\right] \\
&- \frac{ik^3(n-1)(n-2)}{n^2c}\left[\mathbf{Z}_{\mathrm{me}}^{(n-2)} + \mathbf{Z}_{\mathrm{me}}^{(n-2)*}\right] \\
&- \mathbf{S}_{\mathrm{mm}}^{(n)} - \frac{k^2(n-1)}{n^2c^2}\mathbf{S}_{\mathrm{ee}}^{(n-1)} + \frac{k^4(n-1)(n-2)}{n^2}\mathbf{S}_{\mathrm{mm}}^{(n-2)}, \\
\boldsymbol{\tau}_{\mathrm{mxec}}^{(n)} &= -\frac{ik(n-1)}{nc}\left[\mathbf{Z}_{\mathrm{ee}}^{(n-1)} - c^2\mathbf{Z}_{\mathrm{mm}}^{(n-1)*}\right] \\
&- \frac{ik^3(n-1)(n-2)}{n^2c}\left[\mathbf{Z}_{\mathrm{ee}}^{(n-2)*} - c^2\mathbf{Z}_{\mathrm{mm}}^{(n-2)}\right] \\
&+ \mathbf{S}_{\mathrm{em}}^{(n)*} + \frac{k^2(n-1)}{n^2}\mathbf{S}_{\mathrm{em}}^{(n-1)} - \frac{k^4(n-1)(n-2)}{n^2}\mathbf{S}_{\mathrm{em}}^{(n-2)*}, \\
\boldsymbol{\tau}_{\mathrm{exmc}}^{(n)} &= \frac{ik(n-1)}{nc}\left[c^2\mathbf{Z}_{\mathrm{mm}}^{(n-1)} - \mathbf{Z}_{\mathrm{ee}}^{(n-1)*}\right] \\
&+ \frac{ik^3(n-1)(n-2)}{n^2c}\left[c^2\mathbf{Z}_{\mathrm{mm}}^{(n-2)*} - \mathbf{Z}_{\mathrm{ee}}^{(n-2)}\right] + \mathbf{S}_{\mathrm{me}}^{(n)*} \\
&+ \frac{k^2(n-1)}{n^2}\mathbf{S}_{\mathrm{me}}^{(n-1)} - \frac{k^4(n-1)(n-2)}{n^2}\mathbf{S}_{\mathrm{me}}^{(n-2)*}, \qquad \textbf{(A21)}
\end{aligned}$$

where

$$\begin{aligned}
\mathbf{Z}_{\mathrm{ee}}^{(n)} &= \frac{1}{2}[\nabla D_{\mathrm{ee}}^{(n)} - \nabla\times\mathbf{S}_{\mathrm{ee}}^{(n)} - 2ikc\mathrm{Re}\mathbf{S}_{\mathrm{em}}^{(n)}], \\
\mathbf{Z}_{\mathrm{mm}}^{(n)} &= \frac{1}{2}[\nabla D_{\mathrm{mm}}^{(n)} - \nabla\times\mathbf{S}_{\mathrm{mm}}^{(n)} - \frac{2ik}{c}\mathrm{Re}\mathbf{S}_{\mathrm{em}}^{(n)}], \\
\mathbf{Z}_{\mathrm{me}}^{(n)} &= \frac{1}{2}[\nabla D_{\mathrm{me}}^{(n)} - \nabla\times\mathbf{S}_{\mathrm{me}}^{(n)} - \frac{ik}{c}(\mathbf{S}_{\mathrm{ee}}^{(n)} + c^2\mathbf{S}_{\mathrm{mm}}^{(n)})], \\
\mathbf{Z}_{\mathrm{em}}^{(n)} &= \frac{1}{2}[\nabla D_{\mathrm{em}}^{(n)} - \nabla\times\mathbf{S}_{\mathrm{em}}^{(n)} + \frac{ik}{c}(\mathbf{S}_{\mathrm{ee}}^{(n)} + c^2\mathbf{S}_{\mathrm{mm}}^{(n)})]. \qquad \textbf{(A22)}
\end{aligned}$$

Next, we derive the analytic expression for the optical torque exerted on a spherical chiral particle under the illumination of a standing wave, given by

$$\begin{aligned}
&\mathbf{E} = \mathbf{E}_1 + \mathbf{E}_2, \quad \mathbf{B} = \mathbf{B}_1 + \mathbf{B}_2, \quad \mathbf{E}_1 = \mathcal{E}_1 e^{ik\hat{\boldsymbol{k}}_1\cdot\boldsymbol{r}}, \\
&\mathbf{B}_1 = \mathcal{B}_1 e^{ik\hat{\boldsymbol{k}}_1\cdot\boldsymbol{r}}, \quad \mathbf{E}_2 = \mathcal{E}_2 e^{ik\hat{\boldsymbol{k}}_2\cdot\boldsymbol{r}}, \quad \mathbf{B}_2 = \mathcal{B}_2 e^{ik\hat{\boldsymbol{k}}_2\cdot\boldsymbol{r}}, \qquad \textbf{(A23)}
\end{aligned}$$

where $\boldsymbol{r} = x\hat{\boldsymbol{x}} + y\hat{\boldsymbol{y}} + z\hat{\boldsymbol{z}}$. $k = 2\pi/\lambda$ and $\hat{\boldsymbol{k}}_{1,2} = \pm\hat{\boldsymbol{x}}$, respectively, denote the wave number in the background medium and wave vectors. $\mathcal{E}_{1,2} = -\hat{\boldsymbol{z}}$ and $\mathcal{B}_{1,2} = \hat{\boldsymbol{k}}_{1,2}\times\mathcal{E}_{1,2}$ are the complex polarization vectors. In this geometry, the electric field possesses a component solely in the z-direction, while the magnetic field has a component exclusively in the y-direction. Consequently, the field moments in Eq. (A19) can be reduced to

$$\begin{aligned}
&D_{\mathrm{ee}}^{(n)} = -D_{\mathrm{mm}}^{(n)}, \qquad \mathbf{S}_{\mathrm{em}}^{(n)} = \mathbf{S}_{\mathrm{me}}^{(n)} = i\frac{1}{2}\nabla D_{\mathrm{ee}}^{(n)}, \\
&D_{\mathrm{em}}^{(n)} = D_{\mathrm{me}}^{(n)} = 0, \qquad \mathbf{S}_{\mathrm{ee}}^{(n)} = \mathbf{S}_{\mathrm{mm}}^{(n)} = 0. \qquad \textbf{(A24)}
\end{aligned}$$

Substituting Eq. (A24) into $\mathbf{Z}$ vectors which are demonstrated in Eq. (A22), $\mathbf{Z}$ vectors are given by $\mathbf{Z}_{\mathrm{ee}}^{(n)} = \nabla D_{\mathrm{ee}}^{(n)}, \mathbf{Z}_{\mathrm{mm}}^{(n)} = \mathbf{Z}_{\mathrm{me}}^{(n)} = \mathbf{Z}_{\mathrm{em}}^{(n)} = 0$. Thus, $\boldsymbol{\tau}$ vectors in Eq. (A21) are rewritten by $\boldsymbol{\tau}_{\mathrm{exe}}^{(n)} = \boldsymbol{\tau}_{\mathrm{mxm}}^{(n)} = 0$, $\boldsymbol{\tau}_{\mathrm{exmc}}^{(n)} = \boldsymbol{\tau}_{\mathrm{mxec}}^{(n)}$.

Any monochromatic optical field can be expressed as an integral over the spectrum of a homogeneous plane wave. According to Ref. [43], field moments of arbitrary orders in the interfering optical fields can be reduced to their lowest-order counterparts. In the illustration given by Eq. (A23), the right hand in Eq. (A16) can be expressed as

$$\begin{aligned}
\sum_{m=0}^{\lfloor\frac{l-1}{2}\rfloor} h_{l,m}\boldsymbol{\tau}_{\mathrm{exmc}}^{(l-2m)} &= -i\frac{(2l+1)l!}{8l^3(2l+1)!!}\Big[2R_l^{(7)}(x_{12}) - 2R_l^{(6)}(x_{12}) \\
&+ R_l^{(5)}(x_{12}) + R_l^{(4)}(x_{12})\Big]\nabla D_{\mathrm{ee}}^{(1)}, \qquad \textbf{(A25)}
\end{aligned}$$

with $\nabla D_{\mathrm{ee}}^{(1)} = \nabla|\mathbf{E}|^2$. The coefficients R are linear combinations of Legendre polynomials given in Ref. [43]. x_{12} is expressed by $x_{12} = \hat{\boldsymbol{k}}_1\cdot\hat{\boldsymbol{k}}_2 \equiv -1$; thus, the coefficients R can be reduced to a form related only with order l. After some mathematical algebra, the intensity-gradient torque derives from the interplay between chiral multipoles of equal order, i.e., $\langle\mathbf{T}_{\mathrm{rec}}^{x(l)}\rangle$ in Eqs. (A9)–(A14), which can be expressed as

$$\begin{aligned}
\mathbf{T} = \mathbf{T}_{\mathrm{rec}}^{x(l)} &= \sum_{l=1}^{N}\beta^{(l)}\Re(\gamma_{\mathrm{elec}}^{(l)}\gamma_{\mathrm{x}}^{(l)*} - \gamma_{\mathrm{mag}}^{(l)}\gamma_{\mathrm{x}}^{(l)*})\nabla|\mathbf{E}|^2, \\
\beta^{(l)} &= -\frac{1}{32\pi}\frac{(-2)^l(l+1)^2(l-1)!}{l^2(2l-1)!(2l+1)!!}. \qquad \textbf{(A26)}
\end{aligned}$$

The intensity-gradient torque given by Eq. (A26) is dimensionless and actually gives the numerical value of the optical torque in units of $\varepsilon_0E_0^2/k^3\sqrt{\varepsilon_b}$.

APPENDIX B: THE CHIRAL TORQUE

The main result of this paper is the torque associated only with particle chirality, namely chiral torque $\mathbf{T}_{\mathrm{chiral}}^{(l)}$. According to Eqs. (A9)–(A15), chiral torque can be expressed by

$$\begin{aligned}
\langle\mathbf{T}_{\mathrm{chiral}}^{(l)}\rangle &= -\frac{2^l(l+1)k^{2l+1}}{8\pi(2l+1)!}\sum_{m=0}^{\lfloor\frac{l-1}{2}\rfloor}k^{4m}h_{l,m} \\
&\times\{\Im[\eta_{\mathrm{hhc}}^{(l)}\boldsymbol{\tau}_{\mathrm{exe}}^{(l-2m)} + \eta_{\mathrm{hhc}}^{(l)}\boldsymbol{\tau}_{\mathrm{mxm}}^{(l-2m)} + (\eta_{\mathrm{ehc}}^{(l)} - \eta_{\mathrm{mhc}}^{(l)*})\boldsymbol{\tau}_{\mathrm{exmc}}^{(l-2m)} \\
&+ (\eta_{\mathrm{ehc}}^{(l)*} - \eta_{\mathrm{mhc}}^{(l)})\boldsymbol{\tau}_{\mathrm{mxec}}^{(l-2m)}]\} - \frac{1}{2(l-1)!} \\
&\times\sum_{m=0}^{\lfloor\frac{l-1}{2}\rfloor}k^{4m}h_{l,m}\Re[\gamma_x^{(l)}(\boldsymbol{\tau}_{\mathrm{mxec}}^{(l-2m)} - \boldsymbol{\tau}_{\mathrm{exmc}}^{(l-2m)})]. \qquad \textbf{(B1)}
\end{aligned}$$

To derive the field quantities with the Laplacian, a key mathematical trick is as follows:

$$(\boldsymbol{u}\cdot\boldsymbol{v})^{n-1} = \left[1 - \frac{1}{2}(\boldsymbol{u}-\boldsymbol{v})^2\right]^{n-1} = \sum_{j=0}^{n-1}C_{n,j}(k)(\boldsymbol{u}-\boldsymbol{v})^{2j}, \qquad \textbf{(B2)}$$

where $\boldsymbol{u}^2 = \boldsymbol{v}^2 = 1$. The second equality can be derived from the binomial theorem with the coefficient

$$C_{n,j} = \left(\frac{-1}{2}\right)^{(j)} \frac{(n-1)!}{j!(n-1-j)!}, \tag{B3}$$

which can be applied. After some algebra, one can arrive at

$$\begin{aligned}
&D_{\mathrm{ee}}^{(n)} = \left(k^2 + \frac{\Delta}{2}\right)^{(n-1)} D_{\mathrm{ee}}^{(1)}, \quad D_{\mathrm{mm}}^{(n)} = \left(k^2 + \frac{\Delta}{2}\right)^{(n-1)} D_{\mathrm{mm}}^{(1)},\\
&\mathbf{S}_{\mathrm{ee}}^{(n)} = \left(k^2 + \frac{\Delta}{2}\right)^{(n-1)} \mathbf{S}_{\mathrm{ee}}^{(1)}, \quad \mathbf{S}_{\mathrm{mm}}^{(n)} = \left(k^2 + \frac{\Delta}{2}\right)^{(n-1)} \mathbf{S}_{\mathrm{mm}}^{(1)},\\
&\mathbf{S}_{\mathrm{em}}^{(n)} = \left(k^2 + \frac{\Delta}{2}\right)^{(n-1)} \mathbf{S}_{\mathrm{em}}^{(1)}, \qquad \mathbf{S}_{\mathrm{me}}^{(n)} = -\mathbf{S}_{\mathrm{em}}^{(n)*},\\
&\mathbf{P}_{\mathrm{ee}}^{(n)} = \left(k^2 + \frac{\Delta}{2}\right)^{(n-1)} \mathbf{P}_{\mathrm{ee}}^{(1)}, \quad \mathbf{P}_{\mathrm{mm}}^{(n)} = \left(k^2 + \frac{\Delta}{2}\right)^{(n-1)} \mathbf{P}_{\mathrm{mm}}^{(1)}.
\end{aligned} \tag{B4}$$

The physical meaning of dipole moments in Eq. (B4) is quite straightforward: electric intensity $D_{\mathrm{ee}}^{(1)} = |\mathbf{E}|^2$; magnetic intensity $D_{\mathrm{mm}}^{(1)} = |\mathbf{H}|^2$; electric orbital momentum $\mathbf{P}_{\mathrm{ee}}^{(1)} = \Im[\mathbf{E}^* \cdot (\nabla \mathbf{E})]$; magnetic orbital momentum $\mathbf{P}_{\mathrm{mm}}^{(1)} = \Im[\mathbf{H}^* \cdot (\nabla \mathbf{H})]$; electric spin angular momentum $\Im[\mathbf{S}_{\mathrm{ee}}^{(1)}] = \Im[\mathbf{E}^* \times \mathbf{E}]$; magnetic spin angular momentum $\Im[\mathbf{S}_{\mathrm{mm}}^{(1)}] = \Im[\mathbf{H}^* \times \mathbf{H}]$; complex Poynting vector $\mathbf{S}_{\mathrm{em}}^{(1)} = \mathbf{E} \times \mathbf{H}^*$. Substituting these results into Eq. (B1) and performing some tedious mathematical operations, the final result is given in Eq. (4) of main text. The prefactors are as follows:

$$\begin{aligned}
A_{l,m} &= \frac{-2m + l - 1}{l - 2m}, \quad B_{l,m} = \frac{(-2m + l - 1)(-2m + l - 2)}{(l - 2m)^2},\\
M_{l,m} &= -\frac{2^l (l+1)}{8\pi (2l+1)!} h_{l,m}, \qquad N_{l,m} = -\frac{1}{2(n-1)!} h_{l,m}.
\end{aligned} \tag{B6}$$

Funding. National Natural Science Foundation of China (12174076, 12204117, 12274181); National Key Research and Development Program of China (2023YFF0613700); Guangxi Science and Technology Project (2023GXNSFFA026002, 2024GXNSFBA010261, 2021GXNSFDA196001, AD23026117); Open Project of State Key Laboratory of Surface Physics at Fudan University (KF2022_15).

Disclosures. The authors declare no conflicts of interest.

Data Availability. Data underlying the results presented in this paper are not publicly available at this time but may be obtained from the authors upon reasonable request.

REFERENCES

1. J. Ahn, Z. Xu, J. Bang, *et al.*, "Ultrasensitive torque detection with an optically levitated nanorotor," Nat. Nanotechnol. **15**, 89–93 (2020).
2. C. Gonzalez-Ballestero, M. Aspelmeyer, L. Novotny, *et al.*, "Levitodynamics: levitation and control of microscopic objects in vacuum," Science **374**, eabg3027 (2021).
3. J. Millen, T. S. Monteiro, R. Pettit, *et al.*, "Optomechanics with levitated particles," Rep. Prog. Phys. **83**, 026401 (2020).

$$\begin{aligned}
\hat{\mathcal{C}}_{\mathrm{spin}}^{(l)} &= \Re[\eta_{\mathrm{hhc}}^{(l)}] \sum_{m=0}^{\lfloor \frac{l-1}{2} \rfloor} M_{l,\mathrm{m}} \left[\left(k^2 + \frac{\Delta}{2}\right)^{l-2m} - \frac{2(l-2m)^2 - 3(l-2m) + 1}{(l-2m)^2} \left(k^2 + \frac{\Delta}{2}\right)^{l-2m-1} + B_{l,m} \left(k^2 + \frac{\Delta}{2}\right)^{l-2m-2} \right],\\
\hat{\mathcal{C}}_{\mathrm{curl}}^{(l)} &= \Re[\eta_{\mathrm{hhc}}^{(l)}] \sum_{m=0}^{\lfloor \frac{l-1}{2} \rfloor} M_{l,m} \left[2A_{l,m} \left(k^2 + \frac{\Delta}{2}\right)^{l-2m-1} - 2B_{l,m} \left(k^2 + \frac{\Delta}{2}\right)^{l-2m-2} \right],\\
\hat{\mathcal{C}}_{\mathrm{IG}}^{(l)} &= \Re[\eta_{\mathrm{ehc}}^{(l)} - \eta_{\mathrm{mhc}}^{(l)}] \sum_{m=0}^{\lfloor \frac{l-1}{2} \rfloor} M_{l,m} \left[-A_{l,m} \left(k^2 + \frac{\Delta}{2}\right)^{l-2m-1} - B_{l,m} \left(k^2 + \frac{\Delta}{2}\right)^{l-2m-2} \right],\\
\hat{\mathcal{C}}_{\mathrm{PG}}^{(l)} &= 2\Im[\eta_{\mathrm{ehc}}^{(l)} + \eta_{\mathrm{mhc}}^{(l)}] \sum_{m=0}^{\lfloor \frac{l-1}{2} \rfloor} M_{l,m} \left[A_{l,m} \left(k^2 + \frac{\Delta}{2}\right)^{l-2m-1} - B_{l,m} \left(k^2 + \frac{\Delta}{2}\right)^{l-2m-2} \right]\\
&\quad + 2\Re[\gamma_x^{(l)}] \sum_{m=0}^{\lfloor \frac{l-1}{2} \rfloor} N_{l,m} \left[-A_{l,m} \left(k^2 + \frac{\Delta}{2}\right)^{l-2m-1} + B_{l,m} \left(k^2 + \frac{\Delta}{2}\right)^{l-2m-2} \right],\\
\hat{\mathcal{C}}_{\mathrm{PM}}^{(l)} &= 2\Im[\eta_{\mathrm{ehc}}^{(l)} + \eta_{\mathrm{mhc}}^{(l)}] \sum_{m=0}^{\lfloor \frac{l-1}{2} \rfloor} M_{l,m} \left[-\left(k^2 + \frac{\Delta}{2}\right)^{l-2m} - \frac{1}{l-2m} A_{l,m} \left(k^2 + \frac{\Delta}{2}\right)^{l-2m-1} + B_{l,m} \left(k^2 + \frac{\Delta}{2}\right)^{l-2m-2} \right]\\
&\quad + 2\Re[\gamma_x^{(l)}] \sum_{m=0}^{\lfloor \frac{l-1}{2} \rfloor} N_{l,m} \left[\left(k^2 + \frac{\Delta}{2}\right)^{l-2m} + \frac{1}{l-2m} A_{l,m} \left(k^2 + \frac{\Delta}{2}\right)^{l-2m-1} - B_{l,m} \left(k^2 + \frac{\Delta}{2}\right)^{l-2m-2} \right],\\
\hat{\mathcal{C}}_{\mathrm{IPM}}^{(l)} &= 2\Re[\eta_{\mathrm{ehc}}^{(l)} - \eta_{\mathrm{mhc}}^{(l)}] \sum_{m=0}^{\lfloor \frac{l-1}{2} \rfloor} M_{l,m} \left[-\left(k^2 + \frac{\Delta}{2}\right)^{l-2m} + \frac{1}{l-2m} A_{l,m} \left(k^2 + \frac{\Delta}{2}\right)^{l-2m-1} + B_{l,m} \left(k^2 + \frac{\Delta}{2}\right)^{l-2m-2} \right],
\end{aligned} \tag{B5}$$

with

4. X. Li, D. Dan, S. Zavatski, *et al.*, "Optical tweeze-sectioning microscopy for 3D imaging and manipulation of suspended cells," Sci. Adv. **11**, eadx3900 (2025).
5. Y. Dong, Y. Wang, D. He, *et al.*, "Nearfield observation of spin-orbit interactions at nanoscale using photoinduced force microscopy," Sci. Adv. **10**, eadp8460 (2024).
6. J. Chen, J. Ng, Z. Lin, *et al.*, "Optical pulling force," Nat. Photonics **5**, 531–534 (2011).
7. M. Nieto-Vesperinas, J. Sáenz, R. Gómez-Medina, *et al.*, "Optical forces on small magnetodielectric particles," Opt. Express **18**, 11428–11443 (2010).
8. Y. Jiang, H. Chen, J. Chen, *et al.*, "Universal relationships between optical force/torque and orbital versus spin momentum/angular momentum of light," arXiv, arXiv:1511.08546 (2015).
9. Y. Zhou, X. Xu, Y. Zhang, *et al.*, "Observation of high-order imaginary Poynting momentum optomechanics in structured light," Proc. Natl. Acad. Sci. **119**, e2209721119 (2022).
10. Y. Shi, X. Xu, M. Nieto-Vesperinas, *et al.*, "Advances in light transverse momenta and optical lateral forces," Adv. Opt. Photonics **15**, 835–906 (2023).
11. A. Ashkin, J. M. Dziedzic, J. E. Bjorkholm, *et al.*, "Observation of a single-beam gradient force optical trap for dielectric particles," Opt. Lett. **11**, 288–290 (1986).
12. Y. Roichman, B. Sun, Y. Roichman, *et al.*, "Optical forces arising from phase gradients," Phys. Rev. Lett. **100**, 013602 (2008).
13. Y. Jiang, J. Chen, J. Ng, *et al.*, "Decomposition of optical force into conservative and nonconservative components," arXiv, arXiv:1604.05138 (2016).
14. X. Xu and M. Nieto-Vesperinas, "Azimuthal imaginary Poynting momentum density," Phys. Rev. Lett. **123**, 233902 (2019).
15. L. Wei and F. J. Rodríguez-Fortuño, "Optical multipolar torque in structured electromagnetic fields: on helicity gradient torque, quadrupolar torque, and spin of the field gradient," Phys. Rev. B **105**, 125424 (2022).
16. M. Rashid, M. Toroš, A. Setter, *et al.*, "Precession motion in levitated optomechanics," Phys. Rev. Lett. **121**, 253601 (2018).
17. R. Reimann, M. Doderer, E. Hebestreit, *et al.*, "GHz rotation of an optically trapped nanoparticle in vacuum," Phys. Rev. Lett. **121**, 033602 (2018).
18. J. Ahn, Z. Xu, J. Bang, *et al.*, "Optically levitated nanodumbbell torsion balance and GHz nanomechanical rotor," Phys. Rev. Lett. **121**, 033603 (2018).
19. Y. Jin, J. Yan, S. J. Rahman, *et al.*, "6 GHz hyperfast rotation of an optically levitated nanoparticle in vacuum," Photonics Res. **9**, 1344–1350 (2021).
20. Y. Zhao, A. A. Saleh, and J. A. Dionne, "Enantioselective optical trapping of chiral nanoparticles with plasmonic tweezers," ACS Photonics **3**, 304–309 (2016).
21. M. L. Solomon, A. A. Saleh, L. V. Poulikakos, *et al.*, "Nanophotonic platforms for chiral sensing and separation," Acc. Chem. Res. **53**, 588–598 (2020).
22. J. Zhang, T. He, C. Li, *et al.*, "High-speed sorting of sub-20 nm chiral particles via toroidal-enhanced separated potential wells," Nano Lett. **24**, 6539–6547 (2025).
23. K. Y. Bliokh, Y. S. Kivshar, and F. Nori, "Magnetoelectric effects in local light-matter interactions," Phys. Rev. Lett. **113**, 033601 (2014).
24. A. Canaguier-Durand and C. Genet, "Chiral route to pulling optical forces and left-handed optical torques," Phys. Rev. A **92**, 043823 (2015).
25. H. Chen, W. Lu, X. Yu, *et al.*, "Optical torque on small chiral particles in generic optical fields," Opt. Express **25**, 32867–32878 (2017).
26. S. Wang and C. T. Chan, "Lateral optical force on chiral particles near a surface," Nat. Commun. **5**, 3307 (2014).
27. H. Chen, H. Zheng, W. Lu, *et al.*, "Lateral optical force due to the breaking of electric-magnetic symmetry," Phys. Rev. Lett. **125**, 073901 (2020).
28. H. Zheng, H. Chen, J. Ng, *et al.*, "Optical gradient force in the absence of light intensity gradient," Phys. Rev. B **103**, 035103 (2021).
29. S. Kuhn, A. Kosloff, B. A. Stickler, *et al.*, "Full rotational control of levitated silicon nanorods," Optica **4**, 356–360 (2017).
30. Y. Arita, M. Mazilu, and K. Dholakia, "Laser-induced rotation and cooling of a trapped microgyroscope in vacuum," Nat. Commun. **4**, 2374 (2013).
31. X. Li, D. Dan, S. Zavatski, *et al.*, "Optical tweeze-sectioning microscopy for 3D imaging and manipulation of suspended cells," Sci. Adv. **11**, eadx3900 (2025).
32. X. Yuan, J. Min, Y. Zhou, *et al.*, "Optical diffraction tomography based on quadriwave lateral shearing interferometry," Opt. Laser Technol. **177**, 111124 (2024).
33. M. Nieto-Vesperinas and X. Xu, "Reactive helicity and reactive power in nanoscale optics: evanescent waves. Kerker conditions. Optical theorems and reactive dichroism," Phys. Rev. Res. **3**, 043080 (2021).
34. X. Xu, M. Nieto-Vesperinas, Y. Zhou, *et al.*, "Gradient and curl optical torques," Nat. Commun. **15**, 6230 (2024).
35. K. Y. Bliokh, A. Y. Bekshaev, and F. Nori, "Dual electromagnetism: helicity, spin, momentum and angular momentum," New J. Phys. **15**, 033026 (2013).
36. S. Golat, A. J. Vernon, and F. J. Rodríguez-Fortuño, "The electromagnetic symmetry sphere: a framework for energy, momentum, spin and other electromagnetic quantities," arXiv, arXiv:2405.15718 (2024).
37. K. Y. Bliokh, A. Y. Bekshaev, and F. Nori, "Extraordinary momentum and spin in evanescent waves," Nat. Commun. **5**, 3300 (2014).
38. A. Y. Bekshaev, K. Y. Bliokh, and F. Nori, "Transverse spin and momentum in two-wave interference," Phys. Rev. X **5**, 011039 (2015).
39. Y. Zhou, Y. Zhang, X. Xu, *et al.*, "Optical forces on multipoles induced by the Belinfante spin momentum," Laser Photonics Rev. **17**, 2300245 (2023).
40. X. Yu, Y. Li, B. Xu, *et al.*, "Anomalous lateral optical force as a manifestation of the optical transverse spin," Laser Photonics Rev. **17**, 2300212 (2023).
41. M. Nieto-Vesperinas and X. Xu, "The complex Maxwell stress tensor theorem: the imaginary stress tensor and the reactive strength of orbital momentum. A novel scenery underlying electromagnetic optical forces," Light Sci. Appl. **11**, 297 (2022).
42. A. Hayat, J. B. Mueller, and F. Capasso, "Lateral chirality-sorting optical forces," Proc. Natl. Acad. Sci. **112**, 13190–13194 (2015).
43. H. Zheng, X. Li, Y. Jiang, *et al.*, "General formulations for computing the optical gradient and scattering forces on a spherical chiral particle immersed in generic monochromatic optical fields," Phys. Rev. A **101**, 053830 (2020).
44. P. Ju, Y. Jin, K. Shen, *et al.*, "Near-field GHz rotation and sensing with an optically levitated nanodumbbell," Nano Lett. **23**, 10157–10163 (2023).
45. Y. Zhang, C. Min, X. Dou, *et al.*, "Plasmonic tweezers: for nanoscale optical trapping and beyond," Light Sci. Appl. **10**, 59 (2021).
46. T. Zhu, Y. Cao, L. Wang, *et al.*, "Self-induced backaction optical pulling force," Phys. Rev. Lett. **120**, 123901 (2018).
47. H. Li, Y. Cao, B. Shi, *et al.*, "Momentum-topology-induced optical pulling force," Phys. Rev. Lett. **124**, 143901 (2020).
48. Y. Shi, T. Zhu, A. Q. Liu, *et al.*, "Inverse optical torques on dielectric nanoparticles in elliptically polarized light waves," Phys. Rev. Lett. **129**, 053902 (2022).
49. F. Nan, F. J. Rodríguez-Fortuño, S. Yan, *et al.*, "Creating tunable lateral optical forces through multipolar interplay in single nanowires," Nat. Commun. **14**, 6361 (2023).
50. Y. Hu, J. J. Kingsley-Smith, M. Nikkhou, *et al.*, "Structured transverse orbital angular momentum probed by a levitated optomechanical sensor," Nat. Commun. **14**, 2638 (2023).
51. K. Achouri, M. Chung, A. Kiselev, *et al.*, "Multipolar pseudochirality-induced optical torque," ACS Photonics **10**, 3275–3282 (2023).
52. M. Riccardi and O. J. Martin, "Electromagnetic forces and torques: from dielectrophoresis to optical tweezers," Chem. Rev. **123**, 1680–1711 (2023).
53. J. Applequist, "Traceless cartesian tensor forms for spherical harmonic functions: new theorems and applications to electrostatics of dielectric media," J. Phys. A Math. Gen. **22**, 4303 (1989).
54. G. Gouesbet and J. A. Lock, "On the electromagnetic scattering of arbitrary shaped beams by arbitrary shaped particles: a review," J. Quant. Spectrosc. Radiat. Transfer **162**, 31–49 (2015).